



Water Resources Research

RESEARCH ARTICLE

10.1029/2018WR024256

Special Section:

The Energy Exascale Earth System Model (E3SM)

Whitney L. Forbes and Jiafu Mao contributed equally to this work.

Key Points:

- Latest NRNI data, ELM simulations, and river routing model were employed to study the long-term hydrologic changes in CRB
- Significant declines in the CRB June–October streamflow led to an earlier center of timing and significant decreases in annual total, summer mean, and peak streamflow
- The changes in annual total, summer mean, and center of timing of streamflow were mainly attributed to changing climate and variability

Supporting Information:

- Supporting Information S1

Correspondence to:

J. Mao and M. Jin,
maoj@ornl.gov;
jin@utk.edu

Citation:

Forbes, W. L., Mao, J., Ricciuto, D. M., Kao, S.-C., Shi, X., Tavakoly, A. A., et al. (2019). Streamflow in the Columbia River Basin: Quantifying changes over the period 1951–2008 and determining the drivers of those changes. *Water Resources Research*, 55, 6640–6652. <https://doi.org/10.1029/2018WR024256>

Received 12 OCT 2018

Accepted 14 JUL 2019

Accepted article online 27 JUL 2019

Published online 6 AUG 2019

©2019. American Geophysical Union.
All Rights Reserved.

Streamflow in the Columbia River Basin: Quantifying Changes Over the Period 1951–2008 and Determining the Drivers of Those Changes

Whitney L. Forbes^{1,2}, Jiafu Mao² , Daniel M. Ricciuto² , Shih-Chieh Kao² , Xiaoying Shi², Ahmad A. Tavakoly³ , Mingzhou Jin¹ , Weidong Guo^{4,5} , Tianbao Zhao⁶ , Yutao Wang⁷, Peter E. Thornton² , and Forrest M. Hoffman⁸

¹Department of Industrial and Systems Engineering, University of Tennessee, Knoxville, TN, USA, ²Environmental Sciences Division and Climate Change Science Institute, Oak Ridge National Laboratory, Oak Ridge, TN, USA, ³Coastal and Hydraulics Laboratory, U.S. Army Engineer Research and Development Center, Vicksburg, MS, USA, ⁴CMA-NJU Joint Laboratory for Climate Prediction Studies, Institute for Climate and Global Change Research, School of Atmospheric Sciences, Nanjing University, Nanjing, China, ⁵Joint International Research Laboratory of Atmospheric and Earth System Sciences, Nanjing, China, ⁶Key Laboratory of Regional Climate-Environment Research for East Asia, Institute of Atmospheric Physics, Chinese Academy of Sciences, Beijing, China, ⁷Fudan Tyndall Center, Department of Environmental Science and Engineering, Fudan University, Shanghai, China, ⁸Computational Sciences and Engineering Division and Climate Change Science Institute, Oak Ridge National Laboratory, Oak Ridge, TN, USA

Abstract Trend, detection, and attribution analyses were performed using naturalized streamflow observations and routed land surface model runoff for 10 subbasins in the Columbia River Basin during water years 1951–2008. The Energy Exascale Earth System land-surface model (ELM) version 1.0 and the Routing Application for Parallel computation of Discharge (RAPID) routing model were used to conduct semi-factorial simulations driven by multiple sets of bias-corrected forcing data sets. Four main potential drivers, including climate change (CLMT), CO₂ concentration (CO₂), nitrogen deposition (NDEP), and land use and land cover change (LULCC), were analyzed during the assessment. All subbasins showed significant ($\alpha = 0.10$) declines in the observed amount of annual total streamflow, except for the Middle and Upper Snake and Upper Columbia Subbasins. These declines were led by significant decreases in June–October streamflow, which also directly led to significant decreases in peak and summer streamflow. Except for the Snake River Subbasins, LULCC had the same pattern of declines in monthly streamflow, but the period was shifted to May–September. NDEP also had significant trends in June–October; however, rather than decreases, the trends showed significant increases in streamflow. While there were significant trends in CO₂, NDEP, and LULCC, their signals of change were weak in comparison to the signal in CLMT and the natural internal variability found in streamflow. Overall, the detection and attribution analysis showed that the historical changes found in annual total, center of timing of, and summer mean streamflow could be attributed to changing climate and variability.

1. Introduction

Discovering and tracking trends in the hydrological cycle for the western United States has been an important area of research. In a series of studies, Barnett et al. (2008), Bonfils et al. (2008), Pierce et al. (2008), and Hidalgo et al. (2009) conducted detection and attribution (D&A) analyses for multiple hydro-meteorological variables in the western United States (i.e., streamflow availability, center of timing, snowpack, minimum and maximum daily temperature, winter air temperature, frost days, and degree-days above 0 °C). They found that the trends in the respective variables over the period 1950–1999 were at least partially human-induced. Human-induced changes have also been discovered in summer streamflow in the British Columbia (Najafi et al., 2017a). For the Upper Colorado River Basin, Xiao et al. (2018) found that naturalized streamflow over the period 1916–2014 decreased 16.5% despite a 1.4% increase in annual precipitation. They determined that 53% of the decrease was due to warming, while the remaining ~47% was from decreases in winter precipitation (Xiao et al., 2018). More recently, studies have focused on the change in snowpack and precipitation type. Najafi et al. (2017b), in addition to streamflow changes, also attributed declines in the British Columbia spring snowpack to anthropogenic forcings. For the western United States, Mote et al. (2018) found that 33% of snow monitoring sites with observations from 1955 to 2016 had significant

declines in snowpack. Berghuijs et al. (2014) showed that the fraction of annual precipitation falling as snow rather than rain for the period 1948–2001 had significant influence on annual streamflow in the contiguous United States. More specifically, they determined that watersheds with a historically higher percentage of precipitation falling as snow, as opposed to rain, had a higher long-term and interannual mean streamflow. This proportion of precipitation type (i.e., snow versus rain) is more closely linked to temperature variations than to variations in precipitation amount in the western United States (Safeeq et al., 2016). Hence, it is believed that the loss in snowpack is due to warmer winter temperatures leading to more winter precipitation falling as rain rather than as snow (Regonda et al., 2005). Fyfe et al. (2017) projected that future western U.S. snowpack will decline up to another 60% in the next 30 years. The projected climate changes leading to decreases in snowpack also lead to decreases in mountain system groundwater recharge (Meixner et al., 2016). In addition, Barnett et al. (2005) predicted that by 2050, the Columbia River system would not be able to sustain historical levels of both spring and autumn water releases for hydropower generation and releases for spring and summer salmon runs.

Leveraging a newly available naturalized daily streamflow data set from the Bonneville Power Administration (Bonneville Power Administration (BPA), 2017), in this study, we performed a comprehensive D&A analysis of multiple hydrological variables in the Columbia River Basin (CRB) and its subbasins. The CRB is of particular interest due to its significant multipurpose river system benefits in ecology, environment, irrigation, navigation, recreation, flood control, and hydropower generation (Bonneville Power Administration (BPA), 2017). We employed the Energy Exascale Earth System land-surface model (ELM) version 1.0 to simulate the surface hydrology with various forcing data sets. We also took advantage of a recently developed river routing model, Routing Application for Parallel computation of Discharge (RAPID; David, Habets, et al., 2011, David, Maidment, et al., 2011; Snow et al., 2016; Tavakoly et al., 2017), to efficiently route streamflow through over 192,000 NHDPlus (McKay et al., 2012) river segments in the CRB. To investigate both the annual and seasonal streamflow, we focused on the center of timing, summer mean, and peak flow. Quantification of changes in the CRB streamflow metrics were also analyzed due to changing climate and climate variability versus changes in carbon dioxide concentration, nitrogen deposition (NDEP), and land use and land cover change (LULCC). In the simplest terms, excluding storage changes, runoff can be considered as the difference between long-term precipitation and evapotranspiration (Gedney et al., 2014). Changes in carbon dioxide concentration, NDEP, and land use and land cover affect evapotranspiration. Carbon dioxide concentration and NDEP affect vegetation dynamics and associated hydrologic variations of the soil-vegetation system. For example, increasing atmospheric carbon dioxide can lead to stomatal closure, which reduces plant transpiration, whereas NDEP, up to a saturation limit, can lead to increased water uptake due to nitrogen-induced fertilization effect on plants. However, once the nitrogen saturation limit is reached, it can restrict growth, therefore decreasing water uptake of vegetation (Aber et al., 1989). LULCC have the ability to alter evapotranspiration by impacting available energy and/or water, photosynthesis rates, nutrient levels, and land-surface roughness (Sterling et al., 2013). More detailed information, in terms of how these human factors are parameterized to affect the terrestrial hydrology especially the streamflow in land surface models, can be found at Mao et al. (2015) and Shi et al. (2011, 2013). By considering the subbasins within the CRB, spatial variability within these changes were also systematically quantified.

2. Methods

2.1. Data

Three meteorological forcing data sets, including the commonly used CRUNCEP (6-hourly time step), Princeton (3-hourly time step), and the newly released GSWP3 (3-hourly time step) were utilized to drive the offline ELM simulations (van den Hurk et al., 2016). To reduce the biases in these drivers, the widely used Livneh et al. (2013) daily gridded meteorological observations were aggregated to the same 0.5° by 0.5° spatial resolution for bias correction. For each forcing data set during 1951–2008, the subdaily precipitation at each grid was linearly rescaled to match the corresponding Livneh et al. (2013) daily total precipitation. Similarly, the subdaily temperature at each grid was shifted so that they have the same average daily temperature as the Livneh et al. (2013) values. These bias-corrected forcing data sets are denoted as CRUNCEP5-Livneh, GSWP3-Livneh, and Princeton-Livneh for further evaluation and comparison. Even though the Livneh data set has been shown to have cold biases in mountainous regions (Frans et al., 2018; Jiang et al., 2018; Mauger

et al., 2016; River Management Joint Operating Committee, 2018), it provides an improvement over the low precipitation bias found in the CRUNCEP, GSWP3, and Princeton drivers for the CRB region and was chosen to be used for bias correction in the RMJOC-II Part I (River Management Joint Operating Committee, 2018). Other data sets such as Parameter-elevation Regressions on Independent Slopes Model [PRISM] and North American Regional Reanalysis (NARR) could not be used due to their respective lack of spatial and temporal coverage (i.e., PRISM only offers coverage for the contiguous United States and daily values from PRISM and NARR are only available since 1981 and 1979, respectively).

For the streamflow evaluation and model verification, we used the No Regulation No Irrigation (NRNI) data set (Bonneville Power Administration (BPA), 2017). For much hydrologic and geophysical research, unregulated streamflow observations that are free from human influence are typically used. Given the heavy water regulation in CRB, however, many of the gauge observations were influenced by human activities and cannot be used directly to study the changes of historical natural flow. By adding back the first-order influences, such as historical irrigation withdrawal and reservoir regulation, the NRNI data represent one of the closest reconstructions of the CRB natural streamflow. Although secondary effects, such as lake attenuation, return flow lag, and ground water exchange, are not completely addressed, NRNI overall provides a good proxy for the naturalized streamflow conditions. In this study, we began with 179 NRNI stations containing data from July 1928 to September 2008 across both the United States and Canadian portions of the CRB. For analyses, we further selected the farthest downstream gauge stations having satisfactory model performance to represent each of the 10 subbasins within the CRB. A description of the 10 subbasins and the corresponding stations is presented in section 2.3. The results reported here cover the period from October 1950 to September 2008 (i.e., water year 1951–2008). More methodology information about how this data set was produced can be found in River Management Joint Operating Committee (2018).

2.2. Factorial ELM Experiments

Here we use the ELM version 1.0, which is heavily based on the Community Land Model (CLM) version 4.5 (Oleson et al., 2013) and CLM version 4.0 (Lawrence et al., 2011) with notable improvements to include representations of carbon and nutrient storage (Metcalf et al., 2017), phosphorus cycling (Yang et al., 2014), and hydrologic cycling in western U.S. forests (Duarte et al., 2017). Because of the models' mechanistic representation of vegetation and soil processes, ELM and CLM can predict the physiological effects of increasing CO₂, the effects of NDEP on nutrient cycling and vegetation growth, and the impacts of land use change on land surface processes. Therefore, CLM has been used for factorial studies in the past (Mao et al., 2015; Shi et al., 2011, 2013), leading to new insights about the effects of specific anthropogenic forcings on hydrologically relevant model outputs.

We followed the protocol of Multi-scale Synthesis and Terrestrial Model Intercomparison Project (MsTMIP) (Huntzinger et al., 2013) to design and perform a series of ELM simulations for the D&A analysis. A total of 24 semifactorial ELM simulations were produced by using six sets of meteorological forcings at 0.5° by 0.5° spatial resolution. For each of these six meteorological forcing data sets, the carbon and nutrient cycles were equilibrated using the acceleration decomposition method for soil organic matter pools described by Thornton and Rosenbloom (2005). During this spinup phase, we repeatedly cycled the input meteorology over the 1950–1969 period (the first 20 years available in the Livneh data set) and held other forcings at constant 1850 values (i.e., preindustrial values). These spinup simulations provided the initial state for the semifactorial simulations, which all began in the year 1850 and ran through 2008. For the all-factor simulation, all environmental drivers were allowed to vary throughout the fully transient simulation (named ALL). The sources and implementation of selected anthropogenic drivers (e.g., CO₂ concentration [CO₂] and NDEP) are consistent with those in Bonan and Levis (2010). In the climate-only simulation, the climatic factors (e.g., temperature, precipitation, and shortwave radiation) cycled between 1950 and 1969 from model years 1850–1969, then used transient climate from 1970–present day; globally averaged CO₂, NDEP, and land use and land cover were held constant at their 1850 values (named CLMT). The third simulation used transient climate and land use and land cover, while the fourth simulation allowed transient climate, land use and land cover, and CO₂. We used the difference between the third simulation and CLMT to isolate the effect of LULCC, which in our simulation only includes the effects of harvest and changes in plant functional type (PFT) distribution as prescribed by Hurtt et al. (2011). The difference between the fourth and the third simulations is the effect of atmospheric CO₂. To isolate the net effect of NDEP, we used the difference of ALL and

the fourth simulation (named NDEP). Since the radiative and physiological effects of CO₂ on climate change cannot be separated by using offline ELM simulations and are included in the transient climate drivers, CO₂, NDEP, and LULCC thus represent the direct effects of CO₂ physiology, NDEP, and LULCC, respectively (Forbes et al., 2018; Gedney et al., 2014; Mao et al., 2016; Zhu et al., 2016).

Additionally, for the D&A analysis, we utilized all available daily Coupled Model Intercomparison Project Phase 5 (CMIP5) preindustrial control runoff simulations (piControl) with no year-to-year variations in external influences to characterize the impacts of natural internal variability of the climate system on the streamflow changes (Zhu et al., 2016). Each simulation was spatially interpolated into a 0.5° by 0.5° spatial resolution comparable to the ELM factorial simulations. The simulations were then separated into independent contiguous segments (the last 58 years of the transient period that overlap with the observations) resulting in 18, 3, 14, and 8 segments from Canadian Earth System Model version 2 (CanESM2), Commonwealth Scientific and Industrial Research Organisation Mark version 3.6.0 (CSIRO-Mk3.6.0), Model for Interdisciplinary Research on Climate version 5 (MIROC5), and Norwegian Earth System Model 1- Medium Resolution (NorESM1-M), respectively (Table S1 in the supporting information).

2.3. Streamflow Routing

We used the RAPID river routing model to accumulate the ELM simulated runoff through a much higher resolution nongridded river network. The widely used NHDPlus river network was used on the United States side of the CRB, and the river network developed by the U.S. Army Engineer Research and Development Center (Wahl et al., 2016) was used on the Canadian side. Together, they form ~192,000 high resolution CRB river segments. For each of the selected NRNI stations, a river segment was identified to represent RAPID's river network location. Both the ELM and CMIP5 piControl total surface runoff were first remapped to the nearest river segment and then routed through RAPID.

We divided the CRB into 10 subbasins for evaluation (Figure 1). The specific subbasins and representative stations analyzed along with their location (latitude/longitude), estimated drainage area from USGS and NHDPlus and corresponding USGS gauge station number (where applicable), and are listed in Table S2. Note that not all the subbasins are independent of one another. For example, Mid-Columbia includes all the flow from the respective upstream watersheds. The independent subbasins are labeled with an asterisk in Table S2. Although the Bonneville station (BON) has the largest drainage area, we chose The Dalles to represent the Lower Columbia subbasin, and thus, the cumulative flow for the entire CRB. The spatial locations of the downstream stations are shown in Figure 1 along with their relation to the major flow lines and topography within the CRB.

The multimodel ensemble (MME) mean ALL forcing data from the routed ELM simulations driven by CRUNCEP5-Livneh, GSWP3-Livneh, and Princeton-Livneh (ALL MME-Livneh) for each downstream station were compared to the monthly NRNI data and evaluated by the Nash-Sutcliffe Efficiency (NSE) coefficient. The NSE of the log-transformed flow was also calculated. In comparison, the logarithmic version is less sensitive to differences in peak or extreme values (Krause et al., 2005). The ensemble mean of the routed flow performed well overall. Using the classification from Moriasi et al. (2007) for NSE values using monthly data, NSE values >0.75 were considered very good, $0.65 < \text{NSE} \leq 0.75$ were good, $0.5 < \text{NSE} \leq 0.65$ were satisfactory, and ≤ 0.5 were unsatisfactory. For the nonlogarithmic version, Lower and Mid-Columbia were good, Kootenay and Upper Columbia were satisfactory, and Lower, Middle, and Upper Snake, Yakima, Spokane, and Pend Oreille were unsatisfactory. However, all the subbasins except the Upper Snake reproduced well with very good, good, or satisfactory logarithmic NSE values. The improvement in NSE values by using the log-transformed monthly data suggests that the model did not reproduce the peak flow values well. This was confirmed by looking at the NSE values for the individual metrics (i.e., annual totals, annual maximums, center of timing, and summer means) studied. Excluding Upper Snake, Yakima, and Upper Columbia, all of the NSE values for the annual totals were very good. However, for the annual maximums, all the NSE values were unsatisfactory. The numerical NSE values for the downstream stations are listed in Table S3. Although the runoff was originally generated from a coarse grid, given the river network represented by NHDPlus, RAPID was able to generate reasonable monthly streamflow time series for the purpose of this study.

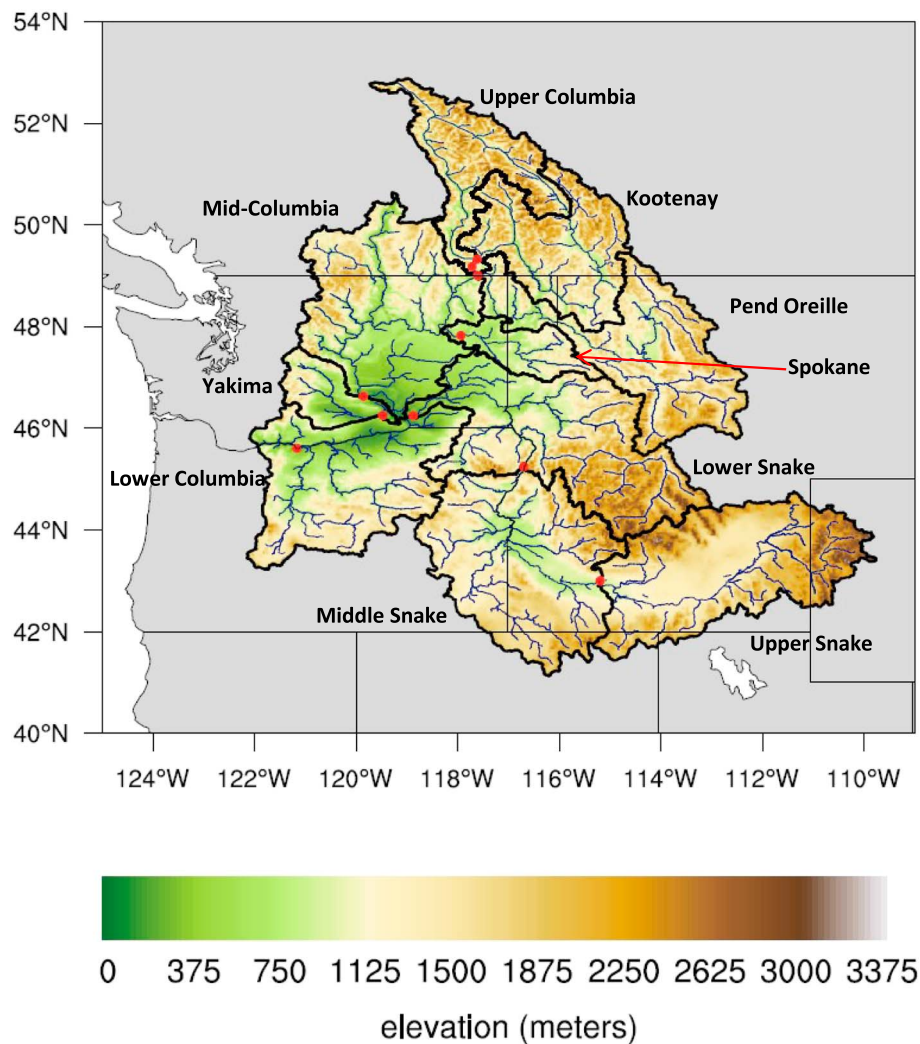


Figure 1. Locations of the major river segments, subbasins, and farthest downstream stations overlapped with the underlying topography.

2.4. Metrics and Methods of Analysis

The following metrics were used to assess the annual and seasonal components of streamflow at each NRNI station location, including annual total flow, annual maximum flow, center of timing, and summer means. For center of timing, we used the center of mass for monthly data as defined in Stewart et al. (2005). Due to the model's ability to more accurately reproduce the monthly streamflow in comparison to the daily flow, we used this definition rather than the day in which half of the annual total flow is exceeded, as has been used in previous studies (Burn, 2008; Hidalgo et al., 2009; Maurer et al., 2007; Rauscher et al., 2008; Regonda et al., 2005; Wenger et al., 2010). Summer was defined as July–September to ensure summer started after the peak of the snowmelt flood each year.

Analyses were performed on the model mean of the three simulations driven by bias-corrected forcings (i.e., CRUNCEP5-Livneh, GSWP3-Livneh, and Princeton-Livneh). Analyses performed using the model mean of the simulations produced using CRUNCEP5, GSWP3, and Princeton are shown in Figure S12 in the supporting information. To assess the trends in the monthly climatologies and the four metrics defined above, the Theil-Sen estimator was used to estimate the slope and the Mann-Kendall test was used to determine the trend under significance level $\alpha = 0.10$ (Kendall, 1975; Mann, 1945; Sen, 1968; Theil, 1950; Burkey, 2006). As in Gudmundsson et al. (2017), we chose to use a correlation analysis as a first stage detection analysis. Pearson correlation coefficients between the observations and each model forcing (i.e., ALL, CLMT, CO2, NDEP, and LULCC) were calculated, and in order to be detected, the correlation between the

observations and a forcing had to be greater than the 97.5th percentile of the correlations between the observations and piControl segments. To form the distribution of correlations between the observations and piControl segments, 10,000 samples (with replacement) of size 3 were taken from the piControl segments, each sample was averaged, and then the correlation between the observations and each averaged sample was calculated. Samples of size 3 were taken to match the ensemble size of the ELM forcings. The more in-depth, nonoptimized version of D&A used in Forbes et al. (2018), which assumes the responses to the forcings are independent and linearly additive, was then implemented using the linear model

$$\mathbf{y} = \boldsymbol{\beta}_{ALL} \mathbf{x}_{ALL} + \boldsymbol{\varepsilon}, \quad (1.1)$$

$$= \boldsymbol{\beta}_{CLMT} \mathbf{x}_{CLMT} + \boldsymbol{\beta}_{CO_2} \mathbf{x}_{CO_2} + \boldsymbol{\beta}_{NDEP} \mathbf{x}_{NDEP} + \boldsymbol{\beta}_{LULCC} \mathbf{x}_{LULCC} + \boldsymbol{\varepsilon}, \quad (1.2)$$

where \mathbf{y} denotes the observations, $\boldsymbol{\beta}_i$ is the scaling factor for forcing i , \mathbf{x}_i is the model response to forcing i , and $\boldsymbol{\varepsilon}$ are the residuals. Before the regression analysis was completed, the observations and model responses to each forcing were centered by removing their respective means. The resulting scaling factors are interpreted as follows: if the estimated scaling factor and its confidence interval do not include zero, a change has been detected, and once a change has been detected, it can be attributed if the estimated scaling factor and its confidence interval include one. Unlike Forbes et al. (2018), uncertainties in the scaling factor estimates were calculated using the 43 piControl segments. Optimization of the signal-to-noise ratio was not used due to the limited number of available piControl segments. Using half of the segments for optimizing the observations and CLMT resulted in similar scaling factor estimates but led to wider uncertainty ranges due to using so few segments in the uncertainty calculation (not shown).

3. Results

3.1. Monthly Climatologies and Trends

The distribution of the monthly climatologies at The Dalles is shown in Figure 2a. For analyzing the monthly climatologies, the peak month was defined as the month with the greatest median and the period of peak flow began (ended) in the month that had a median greater than the previous (respectively, next) month's upper quartile. For the observed river flow, the period of peak flow for The Dalles occurred April–August with the peak flow occurring in June. Similarly, the period of peak flow for all the subbasins started in March or April and ended in July or August with the peak flows occurring in either May or June. The subbasins with peaks ending in August were Lower Columbia (The Dalles), Mid-Columbia, Spokane, Pend Oreille, Kootenay, and Upper Columbia. Spokane, Pend Oreille, Kootenay, and Upper Columbia are the most northern independent subbasins, so the long period of the peak flow from the northern subbasins continued into the downstream subbasins (i.e., Lower and Mid-Columbia). Even though June had the greatest median flow at The Dalles, it had the greatest significant decreasing trend for the period and was the start of significant decreases for the entire June–October season (Figure 2b). This decrease consistently occurred across all the subbasins (Figures S1–S9). These significant decreases also led to significant decreases in the summer means. The only significant increase at The Dalles was in March, and while the other subbasins had an estimated increasing trend for March, only the trends for Kootenay and Upper Columbia were significant (Figures S8–S9). Following the estimated increases in March, April shows a mix of significant and insignificant positive and negative trends across the subbasins. However, all the subbasins but Upper Snake had both a significant or insignificant decrease in May. A shift in the center of timing can be seen by the estimated positive trend in March followed by the estimated negative trend in May/June.

Multiyear monthly trends for CO₂, NDEP, and LULCC at The Dalles are shown in Figure 2c. Unsurprisingly, CO₂ increased in almost every month, and this is true for all subbasins. Just as the observations showed significant decreasing trends for June–October (Figure 2b), LULCC shows the same pattern but also includes May. NDEP has a pattern of significant trends for June–October as well, but rather than decreasing, NDEP had increases. In general, if a subbasin had a significant trend for a particular month in both LULCC and NDEP, they had opposing signs. For most of the subbasins, the strongest positive trend for LULCC was in April and was followed by the strongest negative trend in May or June. However, for NDEP, the strongest negative trend was in March or April and was followed by the strongest positive trend in June. There are a couple other results that are interesting. The first being that specifically for Yakima, LULCC had significant positive trends for November–March. The other is significant negative (positive) trends for LULCC (NDEP)

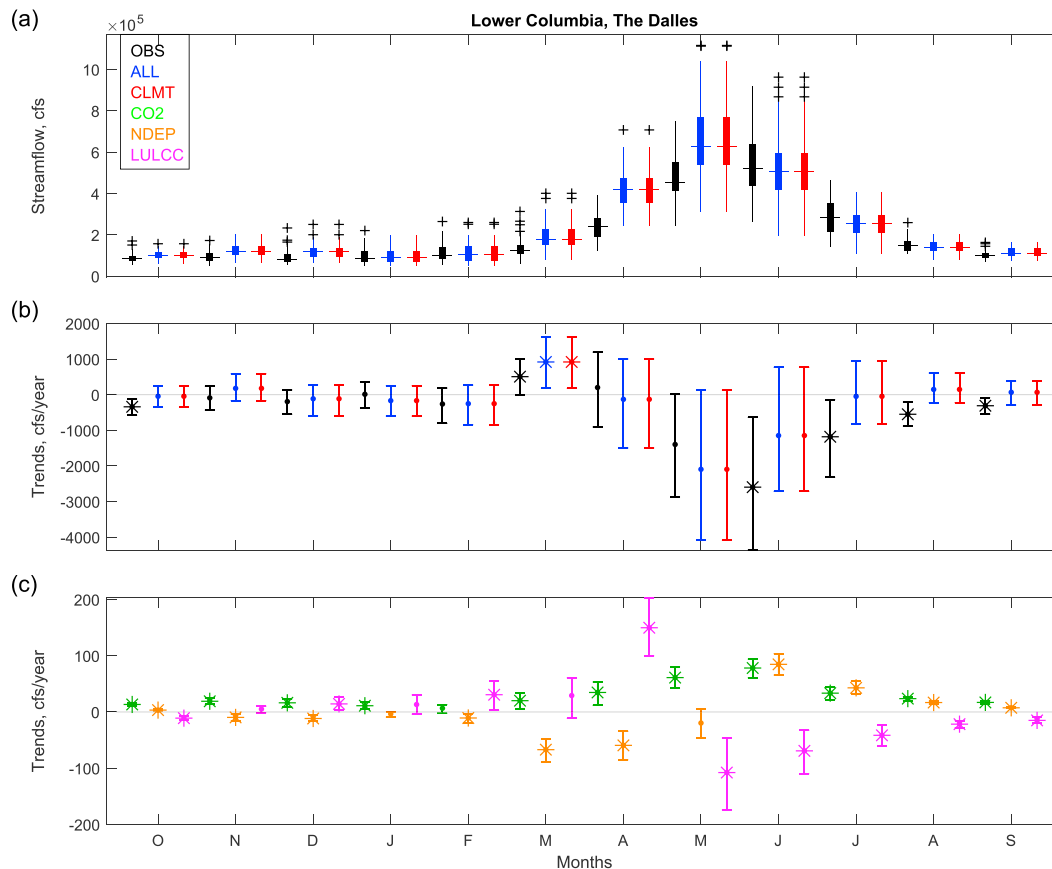


Figure 2. (a) Monthly climatologies for the observations (OBS), ALL, and climate change (CLMT), (b) multiyear trends for the OBS, ALL, and CLMT; and (c) multiyear trends for CO₂ concentration (CO₂), nitrogen deposition (NDEP), and land use and land cover change (LULCC) at The Dalles. Box plots and trends for the observations (black), ALL (blue), and CLMT (red) are shown in figures (a) and (b), respectively. (c) Shows CO₂ (green), NDEP (orange), and LULCC (magenta). For the box plots, the horizontal lines of the box represent the lower quartile, median, and upper quartile. The lines extending from the box represent 1.5 times the interquartile range. Data points outside 1.5 times the interquartile range are outliers and are shown by a “plus” symbol. Trend values and corresponding 90% confidence intervals were estimated using Theil-Sen with significance determined by Mann-Kendall (Burkey, 2006). Significant trends are denoted by the asterisks.

in December and January for Kootenay and Upper Columbia. Figures like Figure 2 for the other subbasins are provided in Figures S1–S9. Figure S10 shows the trend values at each subbasin for the annual totals, annual maximums, center of timing, and summer means.

3.2. D&A Results

The results for the correlation-based detection analysis are shown in Figure 3. As expected, the correlation between the observations and ALL is greater than the 2.5th–97.5th percentile of the correlations between the observations and piControl simulations for all four metrics and all 10 subbasins. Correspondingly, CLMT is detected for all metrics at all subbasins with correlation values approximately equal to those between the observations and ALL. The more informational results come from CO₂, NDEP, and LULCC. For the annual totals, LULCC was detected for Lower Columbia (The Dalles) and upstream throughout the Snake River subbasins. This holds for the annual maximums too but also includes the Mid-Columbia (above Yakima) and Pend Oreille subbasins. The Snake River and Pend Oreille subbasins are the most western subbasins and share borders, so it is possible they are being influenced by the same driver of streamflow changes due to LULCCs. NDEP is also detected for the annual maximums at the Lower Snake, Kootenay, and Upper Columbia subbasins. Other than CLMT, the only detected forcings for center of timing are CO₂ at Mid-Columbia and CO₂ and LULCC at Upper Columbia. For the summer means, CO₂ was detected for all three Snake River subbasins, NDEP was detected for all three Columbia River subbasins, and LULCC was detected for Spokane.

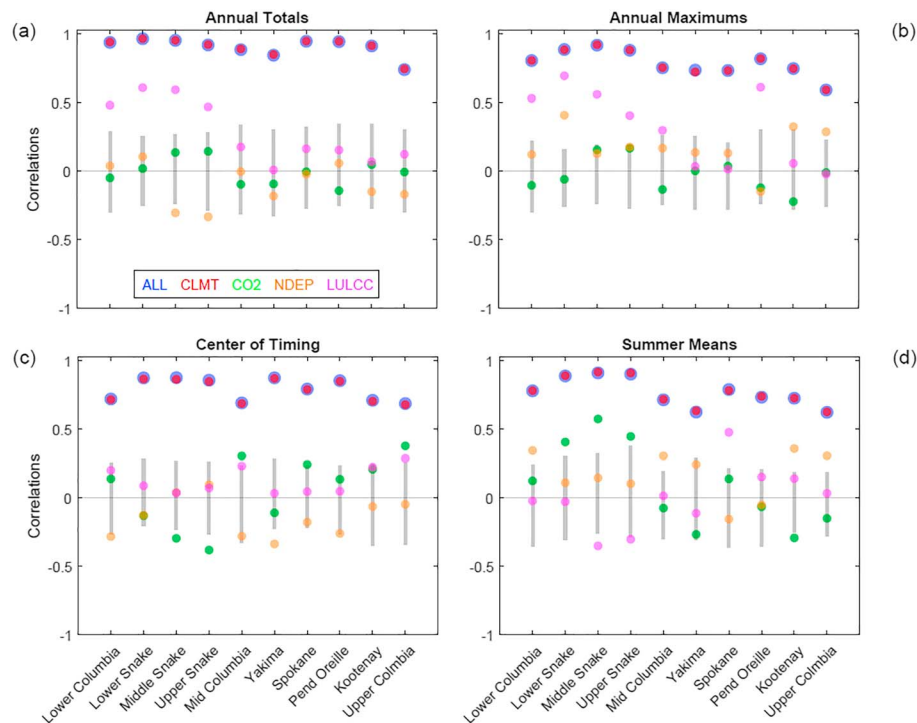


Figure 3. Correlation-Based Detection Analysis for (a) annual totals, (b) annual maximums, (c) center of timing, and (d) summer means for ALL, climate change (CLMT), CO₂ concentration (CO₂), nitrogen deposition (NDEP), and land use and land cover change (LULCC). Pearson correlation coefficients between the observations and ALL (blue), CLMT (red), CO₂ (green), NDEP (orange), and LULCC (magenta) for each subbasin. The light gray lines denote the 2.5th to 97.5th percentiles of the correlations between the observations and the piControl simulations.

D&A results using the linear regression methodology are shown in Figure 4. For annual totals, annual maximums, center of timing, and summer means, 5, 0, 9, and 4 of the 10 subbasins show consistency between ALL and the observations, respectively (Figure 4, right y-axis). Results for the multifactor D&A show the changes in streamflow being detected in CLMT, but for the other forcings, CO₂, NDEP, and LULCC, the scaling factors are too wide to be physically plausible with some of the estimates being completely outside the range -2 to 2. However, rather than only detecting the changes of streamflow in CLMT, the changes can be attributed to CLMT for many cases. More specifically, the changes in annual total streamflow can be attributed to CLMT for all subbasins except for the Upper Snake and Pend Oreille. Only detection of changes in CLMT was achieved for annual maximums due to overestimation in the model simulations, as shown by scaling factors of ALL in Figure 4b. This overestimation is also visible in the monthly figures (Figures 2 and S1–S9). Upper Columbia is the only subbasin for which the change in center of timing cannot be attributed to CLMT. For the summer means, only the changes can be attributed to CLMT for the Lower Columbia (The Dalles), Lower and Middle Snake, and Pend Oreille subbasins. One or more months from the July–August–September summer means were underestimated (overestimated) for the Upper Snake, Mid and Upper Columbia, and Kootenay (Yakima and Spokane) subbasins.

4. Discussion

Direct comparisons to previous D&A studies (e.g., Barnett et al., 2008; Hidalgo et al., 2009; Najafi et al., 2017a) are not possible due to the differences in model forcings studied (i.e., anthropogenic and natural previously vs CLMT, CO₂, NDEP, and LULCC in this paper); however, previous studies have also analyzed the trends in streamflow for the Pacific Northwest including the CRB. The decreases in annual total streamflow shown here were also found in annual mean flow over the period 1948–2006 in Luce and Holden (2009). For individual months, Stewart et al. (2005) looked at the changes in the fraction of annual total flow for 1948–2002. For the stations covering the CRB, they found increases of approximately 3–20% for March and decreases of approximately 10–20% for June, which comprise approximate <10% and 10–30% of the annual total flow, respectively. We found a similar composition and shift in annual flow (Figure 2). Using the

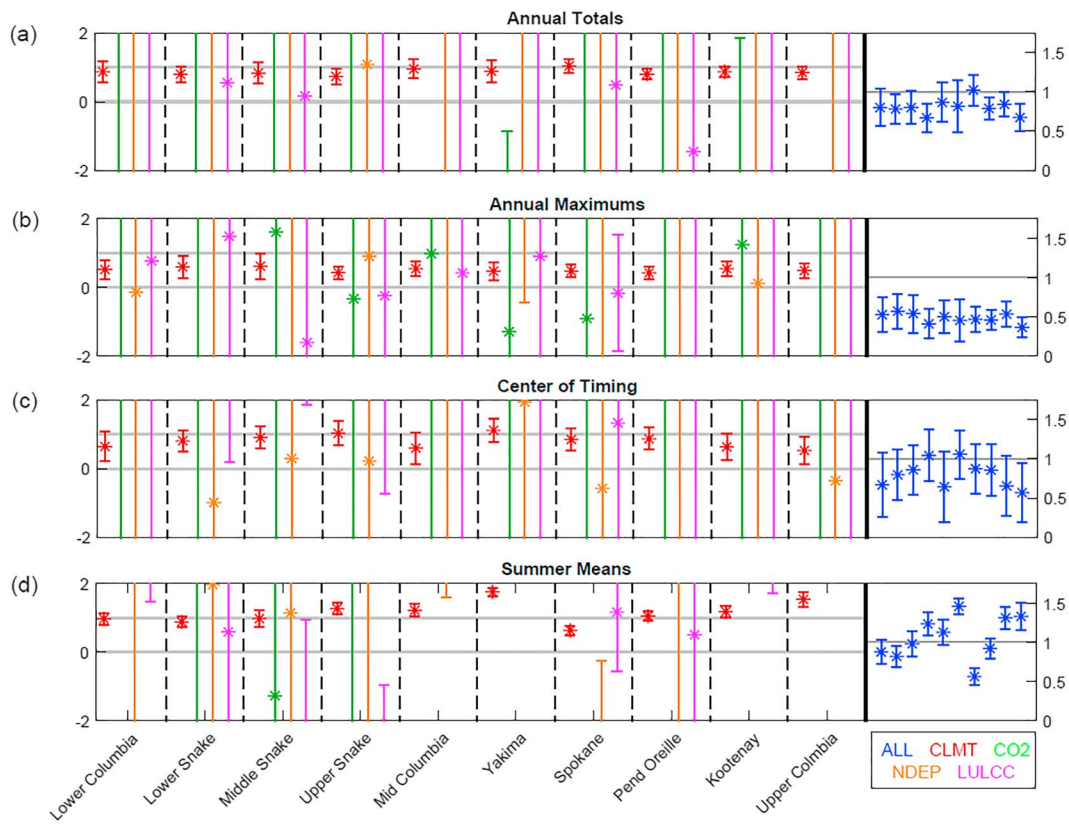


Figure 4. Scaling factor estimates and corresponding 95% confidence intervals for (a) annual totals, (b) annual maximums, (c) center of timing, and (d) summer means using ALL and the linear combination of climate change (CLMT), CO₂ concentration (CO₂), nitrogen deposition (NDEP), and land use and land cover change (LULCC). Scaling factors for CLMT, CO₂, NDEP, and LULCC for each subbasin are shown on the left y-axis in red, green, orange, and magenta, respectively. Scaling factors for the univariate analysis using ALL (blue) are shown on the right y-axis in the same subbasin ordering. The light gray lines denote the values 0 and/or 1.

observational data at The Dalles, March contained 3–11% of the annual total flow during the period 1951–2008, whereas June contained 16–31% (Figure 2). The decline in the fraction of annual total flow in June was consistent with that found in Stewart et al. (2005) at approximately 17%; however, the change in fractional flow for March using the period 1951–2008 was much greater than Stewart et al. (2005), which showed an increase of approximately 45%.

Physiological effects of increased CO₂ may enhance water use efficiency (increasing streamflow through reduced transpiration) but also intensify transpiration by increased leaf area index, causing either positive or negative net effects (Betts et al., 2007). However, the simulated net positive impacts of CO₂ on summertime river flow (Figure 2) were not big enough to counteract the large climate-driven trends. Global-scale analysis like Gedney et al. (2006) indicated that direct CO₂ effects on continental river runoff could be detected and attributed. But for the subbasins in this study, CO₂-induced streamflow changes were not that significant and the observed streamflow decreases could not be attributed to the CO₂ physiological effects.

Beyond the multiyear trends of the monthly climatologies showing a shift to an earlier center of timing and decreased June–October flow in the observations, NDEP and LULCC showed changes in their distributions of flow (Figures 2 and S1–S9). Excluding the Snake River subbasins, the decreasing trends within the observations for June–September were also found in LULCC. Unlike the observations, a shift in flow from May to April is more prominent in LULCC with 7 of the 10 subbasins having significant increasing in April and significant decreasing in May. Also, the effects of LULCC on streamflow caused a positive (negative) trend in the amount of flow for Yakima during November–March (May–September). While all of the subbasins with significant changes in streamflow due to LULCC also had significant shifts from/to tree, grass, and crop PFTs (e.g., from tree to grass or from grass to tree), the shifts in PFTs were not consistent across the subbasins (Figure S11). There was an overall increase in trees but increases/decreases in grasses and crops varied

within the subbasins. For example, the significant changes in grasses for the Pend Oreille subbasin are split with approximately half increasing and half decreasing. The increase in trees would have led to lower albedo in winter, which would have caused more melting of snowpack, and thus, a greater volume of streamflow. For NDEP, the pattern of significance in the observations and LULCC in June–September is present, but rather than having significant decreases, NDEP increased. Contrasting seasonal trends in streamflow by ELM due to NDEP could imply that the observed NDEP effects in these subbasins shifted the vegetation phenology and associated soil water condition, causing positive trends in streamflow in spring and negative changes in the summer and fall. If this happened in reality, the NDEP-induced streamflow increases could suggest the nitrogen saturation limit for the region and month had been met, and rather than increased vegetation growth due to nitrogen fertilization, the nitrogen level is restricting growth (Aber et al., 1989). With respect to the volume of the monthly streamflows, it should be noted that of all the significant trends found in CO₂, NDEP, and LULCC, the strongest trend was equivalent to approximately a 2% change in the respective monthly median volume of ALL.

The differences between the observations and the model simulated streamflow shown in the monthly climatologies and trends are also present in the D&A results. The largest disagreement was found between the annual maximum flow. The simulation consistently overestimated the peak value (Figures 2 and S1–S9). Thus, the scaling factors between the observations and ALL were less than one. For some of the subbasins, the July, August, and/or September flow was overestimated or underestimated and the trend was in the opposing direction (Figures 2 and S1–S9). CLMT was detected using both the correlation-based detection analysis and the regression-based detection methodology; however, the detection of change in CO₂, NDEP, and LULCC for some subbasins using the correlation-based methodology was not reproduced using the regression-based methodology. While both methodologies compare the shape and strength of the pattern of change, the correlation-based methodology does not take scale into account. Thus, even though the pattern of change in CO₂, NDEP, or LULCC may correlate more closely with the observations than the observations correlated with the piControl runs, the magnitudes are much smaller than those found in the observations, ALL, and CLMT.

The main limitation in the previous paper (Forbes et al., 2018) was the bias in the CRUNCEP precipitation driver used in the MsTMIP land surface model simulations. That limitation was overcome in this study by correcting the driver using the temperature and precipitation from Livneh et al. (2013) and by using two more meteorological drivers. To ensure that the reported cold bias from the Livneh data set (Frans et al., 2018) would not affect the overall findings, additional analyses were performed. First, the monthly total precipitation and average temperature for the entire U.S. Pacific Northwest Region (R17) from CRUNCEP5, Livneh, and Daymet V3 (Thornton et al., 2018) were compared. Figure S12 shows that the low precipitation bias within CRUNCEP5 is more prominent than the cold bias within Livneh. The second analysis was completed using data from the 10 subbasins. MME means were calculated from three sets of the satellite-phenology version of the ELM simulations: uncorrected (CRUNCEP5, GSWP3, and Princeton), corrected using temperature and precipitation from Livneh, and corrected using temperature, precipitation, specific humidity, and shortwave radiation from Daymet V3. The annual total, annual maximum, center of timing, and summer mean MME mean time series were plotted along with the observations for each subbasin in Figures S12–S22. In addition to plotting the time series, the centered MME mean time series were compared to the centered observations using the NSE coefficient. The plots showed that the simulations produced using the uncorrected drivers resulted in lower volumes of flow. Additionally, the NSE coefficients generally showed that the simulations produced using Livneh attained a higher level of accuracy than the uncorrected simulations when compared to the observations. Based on these analyses, it was concluded that the cold biases within the Livneh temperature driver did not have a significant impact on the simulations produced for this study. This should be mainly due to the coarse model resolution and large-scale perspective of this study. The regression-based D&A analysis was repeated using the MME mean of the simulations produced without the Livneh correction and is shown in Figure S23. In comparison to the Livneh results (Figure 4), the only metric for which ALL was more consistent with the observations is the annual maximums. It is difficult for models to reproduce minimum and maximum flow data, especially when using a 0.5° by 0.5° spatial resolution. However, given that the simulations produced without the Livneh correction were able to more accurately reproduce the annual maximums, this could be an indication of the cold biases introduced by the Livneh temperature data (Frans et al., 2018) slowing down snowmelt in the model simulation.

For this paper, the main limitation was the limited availability of daily CMIP5 piControl simulations of runoff, which were at least 58 years in length. In total, only 43 independent segments were available. So rather than using half of the segments for prewhitening the observations, ALL, and CLMT and the other half for estimating the uncertainty in the scaling factors, all 43 segments were used in estimating the scaling factor uncertainty. Analysis performed using the prewhitening led to approximately the same scaling factor estimates for ALL and CLMT, but the limited number of segments available for calculating the uncertainty of these estimates led to wider confidence intervals (not shown). Using CMIP5 piControl simulations to drive ELM, rather than routed CMIP5 piControl simulations of runoff, was another possibility for simulating an estimate of the internal variability. Similarly, Barnett et al. (2008) used piControl simulations to drive the variable infiltration capacity model. This type of methodology, however, also introduces inaccuracies due to the lack of feedbacks between the climate system and the land hydrologic components. The other limitation is due to the semi-factorial experimental framework used by the land surface modeling community. Due to this design, CLMT contains both the effects of climate and the indirect effects of CO₂ (e.g., the CO₂ radiative effects), NDEP, and LULCC. Using the factorial fully coupled Earth system model simulations (e.g., those from the CMIP6), which clearly consider the contributions from individual external forcings, their interactive effects, and the internal variations, would be the future direction for regional streamflow D&A studies. This, however, presents a new set of challenges, in terms of much more computational hours involved than the offline runs, no consistent river routing models, and no direct feedback from streamflow to the climate system.

5. Conclusions

On average, the annual total streamflow for the CRB decreased by approximately 15% between 1951 and 2008 (i.e., the percentage of change in volume over time). Of that 15%, roughly 77% was during the June–October months with 40% solely in June (peak flow) and 31% in July–September (summer mean). More specifically, flow in June has declined by 28% on average. The fact that these declines are in five consecutive months during the year is particularly worrisome for all of the inhabitants and the natural ecosystem of this region. On average, these five months provided 49% of the annual total flow with June providing 22% itself. While the CRB does have large reservoirs such as Mica and Grand Coulee, these reservoirs need to balance a variety of competing objectives. During summer months, one main function is reserving space for flood risk management so these CRB reservoirs cannot be simply used to hold and distribute more water during the second half of the year. Other than supplying municipal water sources, which accounts for only a small fraction of the water storage, the lack of water during the second half of the year could also affect the amount of water for irrigation, summer salmon runs, and power generation. The most northern subbasin is Upper Columbia. This subbasin also has the highest elevation. Thus, it is the most heavily impacted by warming winters, which lead to decreased snowpack and center of timing changes. On average, the Upper Columbia saw an increase of 41% and 31% in March and April, respectively, though these months accounted for only about 9% of the total annual flow. Alternatively, June accounted for 25% of the total annual flow and declined by 17%. The D&A analysis shows that these changes in annual total, center of timing, and summer mean streamflow can be attributed to changing climate and variability. Some of the patterns in streamflow changes due to CO₂, NDEP, and LULCC were detected using the correlation-based analysis, but the signals were not strong enough to be detected using the regression-based analysis. So, while the patterns of change within the streamflow changes due to CO₂, nitrogen deposition, and LULCCs are, in some cases, similar to the pattern found in the observations, the magnitude of their contribution to the total flow is very small in comparison to the flow from climate change effects.

References

- Aber, J. D., Nadelhoffer, K. J., Steudler, P., & Melillo, J. (1989). Nitrogen saturation in northern forest ecosystems. *BioScience*, 39(6), 378–386. <https://doi.org/10.2307/1311067>
- Barnett, T. P., Adam, J. C., & Lettenmaier, D. P. (2005). Potential impacts of a warming climate on water availability in snow-dominated regions. *Nature*, 438(7066), 303–309. <https://doi.org/10.1038/nature04141>
- Barnett, T. P., Pierce, D. W., Hidalgo, H. G., Bonfils, C., Santer, B. D., Das, T., et al. (2008). Human-induced changes in the hydrology of the Western United States. *Science*, 319(5866), 1080–1083. <https://doi.org/10.1126/science.1152538>
- Berghuijs, W. R., Woods, R. A., & Hrachowitz, M. (2014). A precipitation shift from snow towards rain leads to a decrease in streamflow. *Nature Climate Change*, 4(7), 583–586. <https://doi.org/10.1038/nclimate2246>

Acknowledgments

This work is supported by the Terrestrial Ecosystem Science Scientific Focus Area (TES SFA) project funded through the Terrestrial Ecosystem Science Program, partially supported by the Reducing Uncertainties in Biogeochemical Interactions through Synthesis and Computing Scientific Focus Area (RUBISCO SFA) project funded through the Regional and Global Climate Modeling Program, and partially supported by the Energy Exascale Earth System Model (E3SM) project funded through the Earth System Modeling Program, in the Climate and Environmental Sciences Division (CESD) of the Biological and Environmental Research (BER) Program in the U.S. Department of Energy Office of Science. This research used resources of the Oak Ridge Leadership Computing Facility at the Oak Ridge National Laboratory, which is supported by the Office of Science of the U.S. Department of Energy under contract DE-AC05-00OR22725. Relevant ELM simulations will be shared at <https://daac.ornl.gov> when this paper is published.

- Betts, R. A., Boucher, O., Collins, M., Cox, P. M., Falloon, P. D., Gedney, N., et al. (2007). Projected increase in continental runoff due to plant responses to increasing carbon dioxide. *Nature*, *448*(7157), 1037–1041. <https://doi.org/10.1038/nature06045>
- Bonan, G., & Levis, S. (2010). Quantifying carbon-nitrogen feedbacks in the Community Land Model (CLM4). *Geophysical Research Letters*, *37*, L07401. <https://doi.org/10.1029/2010GL042430>
- Bonfils, C., Santer, B. D., Pierce, D. W., Hidalgo, H. G., Bala, G., Das, T., et al. (2008). Detection and attribution of temperature changes in the mountainous western United States. *Journal of Climate*, *21*(23), 6404–6424. <https://doi.org/10.1175/2008JCLI2397.1>
- Bonneville Power Administration (BPA) (2017). No Regulation No Irrigation flows (1929 – 2008). Available online at: <https://www.bpa.gov/p/Power-Products/Historical-Streamflow-Data/Pages/No-Regulation-No-Irrigation-Data.aspx>
- Burkey, J. (2006). *A non-parametric monotonic trend test computing Mann-Kendall Tau, Tau-b, and Sens Slope written in Mathworks-MATLAB implemented using matrix rotations*. Seattle, Washington, USA: King County, Department of Natural Resources and Parks, Science and Technical Services section. <http://www.mathworks.com/matlabcentral/fileexchange/authors/23983>
- Burn, D. H. (2008). Climatic influences on streamflow timing in the headwaters of the Mackenzie River Basin. *Journal of Hydrology*, *352*(1-2), 225–238. <https://doi.org/10.1016/j.jhydrol.2008.01.019>
- David, C. H., Habets, F., Maidment, D. R., & Yang, Z. -L. (2011). RAPID applied to the SIM-France model. *Hydrological Processes*, *25*(22), 3412–3425. <https://doi.org/10.1002/hyp.8070>
- David, C. H., Maidment, D. R., Niu, G. -Y., Yang, Z. -L., Habets, F., & Eijkhout, V. (2011). River network routing on the NHDPlus dataset. *Journal of Hydrometeorology*, *12*(5), 913–934. <https://doi.org/10.1175/2011JHM1345.1>
- Duarte, H. F., Raczka, B. M., Ricciuto, D. M., Lin, J. C., Koven, C. D., Thornton, P. E., et al. (2017). Evaluating the Community Land Model (CLM4.5) at a coniferous forest site in northwestern United States using flux and carbon-isotope measurements. *Biogeosciences*, *14*(18), 4315–4340. <https://doi.org/10.5194/bg-14-4315-2017>
- Forbes, W. L., Mao, J., Jin, M., Kao, S. C., Fu, W., Shi, X., et al. (2018). Contribution of environmental forcings to US runoff changes for the period 1950 – 2010. *Environmental Research Letters*, *13*(5), 054023. <https://doi.org/10.1088/1748-9326/aabb41>
- Frans, C., Istanbuloglu, E., Lettenmaier, D. P., Fountain, A. G., & Riedel, J. (2018). Glacier Recession and the Response of Summer Streamflow in the Pacific Northwest United States, 1960–2009. *Water Resources Research*, *54*, 6202–6225. <https://doi.org/10.1029/2017WR021764>
- Fyfe, J. C., Derksen, C., Mudryk, L., Flato, G. M., Santer, B. D., Swart, N. C., et al. (2017). Large near-term projected snowpack loss over the western United States. *Nature Communications*, *8*(1), 14996. <https://doi.org/10.1038/ncomms14966>
- Gedney, N., Cox, P. M., Betts, R. A., Boucher, O., Huntingford, C., & Stott, P. A. (2006). Detection of a direct carbon dioxide effect in continental river runoff records. *Nature*, *439*(7078), 835–838. <https://doi.org/10.1038/nature04504>
- Gedney, N., Huntingford, C., Weedon, G. P., Bellouin, N., Boucher, O., & Cox, P. M. (2014). Detection of solar dimming and brightening effects on Northern Hemisphere river flow. *Nature Geoscience*, *7*(11), 796–800. <https://doi.org/10.1038/ngeo2263>
- Gudmundsson, L., Seneviratne, S. I., & Zhang, X. (2017). Anthropogenic climate change detected in European renewable freshwater resources. *Nature Climate Change*, *7*(11), 813–816. <https://doi.org/10.1038/NCLIMATE3416>
- Hidalgo, H. G., Das, T., Dettinger, M. D., Cayan, D. R., Pierce, D. W., Barnett, T. P., et al. (2009). Detection and attribution of streamflow timing changes to climate change in the Western United States. *Journal of Climate*, *22*(13), 3838–3855. <https://doi.org/10.1175/2009JCLI2470.1>
- Huntzinger, D. N., Schwalm, C., Michalak, A. M., Schaefer, K., King, A. W., Wei, Y., et al. (2013). The North American Carbon Program (NACP) Multi-scale Synthesis and Terrestrial Model Intercomparison Project (MsTMIP): Part I—Overview and experimental design. *Geoscientific Model Development*, *6*(6), 2121–2133. <https://doi.org/10.5194/gmd-6-2121-2013>
- Hurt, G. C., Chini, L. P., Frolking, S., Betts, R. A., Feddema, J., Fischer, G., et al. (2011). Harmonization of land-use scenarios for the period 1500–2100: 600 years of global gridded annual land-use transitions, wood harvest, and resulting secondary lands. *Climatic Change*, *109*(1-2), 117–161. <https://doi.org/10.1007/s10584-011-0153-2>
- Jiang, Y., Kim, J. B., Still, C. J., Kearns, B. K., Kline, J. D., & Cunningham, P. G. (2018). Inter-comparison of multiple statistically downscaled climate datasets for the Pacific Northwest, USA. *Scientific Data*, *5*, 180016(1). <https://doi.org/10.1038/sdata.2018.16>
- Kendall, M. G. (1975). *Rank correlation methods*. London: Griffin.
- Krause, P., Boyle, D. P., & Base, F. (2005). Comparison of different efficiency criteria for hydrological model assessment. *Advances in Geosciences*, *5*, 89–97. <https://doi.org/10.5194/adgeo-5-89-2005>
- Lawrence, D. M., Oleson, K. W., Flanner, M. G., Thornton, P. E., Swenson, S. C., Lawrence, P. J., et al. (2011). Parameterization improvements and functional and structural advances in Version 4 of the Community Land Model. *Journal of Advances in Modeling Earth Systems*, *3*, M03001. <https://doi.org/10.1029/2011MS00045>
- Livneh, B., Rosenberg, E. A., Lin, C., Mishra, V., Andreadis, K., Maurer, E. P., & Lettenmaier, D. P. (2013). A long-term hydrologically based dataset of land surface fluxes and states for the conterminous United States: update and extensions. *Journal of Climate*, *26*(23), 9384–9392. <https://doi.org/10.1175/JCLI-D-12-00508.1>
- Luce, C. H., & Holden, Z. A. (2009). Declining annual streamflow distributions in the Pacific Northwest United States, 1948 – 2006. *Geophysical Research Letters*, *36*, L16401. <https://doi.org/10.1029/2009GL039407>
- Mann, H. B. (1945). Non-parametric test against trend. *Econometrica*, *13*, 245–259.
- Mao, J., Fu, W., Shi, X., Ricciuto, D. M., Fisher, J. B., Dickinson, R. E., et al. (2015). Disentangling climatic and anthropogenic controls on global terrestrial evapotranspiration trends. *Environmental Research Letters*, *10*(9), 094008. <https://doi.org/10.1088/1748-9326/10/9/094008>
- Mao, J., Ribes, A., Yan, B., Shi, X., Thornton, P. E., Séférian, R., et al. (2016). Human-induced greening of the northern extratropical land surface. *Nature Climate Change*, *6*(10), 959–963. <https://doi.org/10.1038/nclimate3056>
- Mauger, G. M., Lee, S.-E., Bandaragoda, C., Serra, Y., & Won, J. (2016). *Effect of climate change on the hydrology of the Chehalis Basin. Climate impacts group*, (p. 53pp. Available online at). Seattle, WA: University of Washington. <http://chehalisbasinstrategy.com/wp-content/uploads/2016/09/Mauger-et-al-2016-Effects-of-Climate-Change.pdf>
- Maurer, E. P., Stewart, I. T., Bonfils, C., Duffy, P. B., & Cayan, D. R. (2007). Detection, attribution, and sensitivity of trends toward earlier streamflow in the Sierra Nevada. *Journal of Geophysical Research*, *112*, D11118. <https://doi.org/10.1029/2006JD008088>
- McKay, L., T. Bondelid, T. Dewald, J. Johnston, R. Moore, and A. Rea (2012). NHDPlus Version 2: User Guide, available at: ftp://ftp.horizon-systems.com/NHDplus/NHDPlusV21/Documentation/NHDPlusV2_User_Guide.pdf
- Meixner, T., Manning, A. H., Stonestrom, D. A., Allen, D. M., Ajami, H., Blasch, K. W., et al. (2016). Implications of projected climate change for groundwater recharge in the western United States. *Journal of Hydrology*, *534*, 124–138. <https://doi.org/10.1016/j.jhydrol.2015.12.027>

- Metcalfe, D. B., Ricciuto, D., Palmroth, S., Campbell, C., Hurry, V., Mao, J., et al. (2017). Informing climate models with rapid chamber measurements of forest carbon uptake. *Global Change Biology*, 23(5), 2130–2139. <https://doi.org/10.1111/gcb.13451>
- Moriari, D. N., Arnold, J. G., Van Liew, M. W., Bingner, R. L., Harmel, R. D., & Veith, T. L. (2007). Model evaluation guidelines for systematic quantification of accuracy in watershed simulations. *Transactions of the ASABE*, 50(3), 885–900. <https://doi.org/10.13031/2013.23153>
- Mote, P. W., Li, S., Lettenmaier, D. P., Xiao, M., & Engel, R. (2018). Dramatic declines in snowpack in the western US. *npj Climate and Atmospheric Science*, 1, Article 2(1). <https://doi.org/10.1038/s41612-018-0012-1>
- Najafi, M. R., Zweirs, F., & Gillet, N. (2017a). Attribution of the observed spring snowpack decline in British Columbia to anthropogenic climate change. *Journal of Climate*, 30(11), 4113–4130. <https://doi.org/10.1175/JCLI-D-16-0189.1>
- Najafi, M. R., Zweirs, F. W., & Gillet, N. P. (2017b). Attribution of observed streamflow changes in key British Columbia drainage basins. *Geophysical Research Letters*, 44, 11,012–11,020. <https://doi.org/10.1002/2017GL075016>
- Oleson, K. W., Lawrence, D. M., Bonam, G. R., Flanner, M. G., Kluzek, E., Lawrence, P. J., et al. (2013). Technical description of version 4.5 of the Community Land Model (CLM). N. C. f. A. Research. NCAR Technical Note NCAR/TN-503+STR (422 pp.). Boulder, CO. <https://doi.org/10.5065/D6FB50WZ>
- Pierce, D. W., Barnett, T. P., Hidalgo, H. G., Das, T., Bonfils, C., Santer, B. D., et al. (2008). Attribution of declining Western U.S. snowpack to human effects. *Journal of Climate*, 21(23), 6425–6444. <https://doi.org/10.1175/2008JCLI2405.1>
- Rauscher, S. A., Pal, J. S., Duffenbaugh, N. S., & Benedetti, M. M. (2008). Future changes in snowmelt-driven runoff timing over the western US. *Geophysical Research Letters*, 35, L16703. <https://doi.org/10.1029/2008GL034424>
- Regonda, S. K., Rajagopalan, B., Clark, M., & Pitlick, J. (2005). Seasonal cycle shifts in hydroclimatology over the western United States. *Journal of Climate*, 18(2), 372–384. <https://doi.org/10.1175/JCLI-3272.1>
- River Management Joint Operating Committee. (2018). Climate and hydrology datasets for RMJOC long-term planning studies: Second edition (RMJOC-II) Part I: Hydroclimate projections and analyses. Available on line at: <https://www.bpa.gov/p/Generation/Hydro/hydro/cc/RMJOC-II-Report-Part-I.pdf>
- Safeeq, M., Shukla, S., Arismendi, I., Grant, G. E., Lewis, S. L., & Nolin, A. (2016). Influence of winter season climate variability on snow-precipitation ratio in the western United States. *International Journal of Climatology*, 36(9), 3175–3190. <https://doi.org/10.1002/joc.4545>
- Sen, P. K. (1968). Estimates of the Regression Coefficient Based on Kendall's Tau. *Journal of the American Statistical Association*, 63(324), 1379–1389. <https://doi.org/10.1080/01621459.1968.10480934>
- Shi, X., Mao, J., Thornton, P. E., Hoffman, F. M., & Post, W. M. (2011). The impact of climate, CO₂, nitrogen deposition and land use change on simulated contemporary global river flow. *Geophysical Research Letters*, 38, L08704. <https://doi.org/10.1029/2011GL046773>
- Shi, X., Mao, J., Thornton, P. E., & Huang, M. (2013). Spatiotemporal patterns of evapotranspiration in response to multiple environmental factors simulated by the community land model. *Environmental Research Letters*, 8(2), 024012. <https://doi.org/10.1088/1748-9326/8/2/024012>
- Snow, A. D., Christensen, S. D., Swain, N. R., Nelson, E. J., Ames, D. P., Jones, N. L., et al. (2016). A high-resolution national-scale hydrologic forecast system from a global ensemble land surface model. *Journal of the American Water Resources Association*, 52(4), 950–964. <https://doi.org/10.1111/1752-1688.12434>
- Sterling, S. M., Ducharme, A., & Polcher, J. (2013). The impact of global land-cover change on the terrestrial water cycle. *Nature Climate Change*, 3(4), 385–390. <https://doi.org/10.1038/nclimate1690>
- Stewart, I. T., Cayan, D. R., & Dettinger, M. D. (2005). Changes toward earlier streamflow timing across western North America. *Journal of Climate*, 18(8), 1136–1155. <https://doi.org/10.1175/JCLI3321.1>
- Tavakoly, A. A., Snow, A. D., David, C. H., Follum, M. L., Maidment, D. R., & Yang, Z. -L. (2017). Continental-scale river flow modeling of the Mississippi River Basin using high-resolution NHDPlus dataset. *Journal of the American Water Resources Association*, 53(2), 258–279. <https://doi.org/10.1111/1752-1688.12456>
- Theil, H. (1950). A rank-invariant method of linear and polynomial regression analysis, I, II, III. Proceedings of the Koninklijke Nederlandse Akademie van Wetenschappen, 53, 386–392, 521–525, 1397–1412.
- Thornton, P. E., & Rosenbloom, N. A. (2005). Ecosystem model spin-up: Estimating steady state conditions in a coupled terrestrial carbon and nitrogen cycle model. *Ecological Modelling*, 189(1–2), 25–48. <https://doi.org/10.1016/j.ecolmodel.2005.04.008>
- Thornton, P. E., Thornton, M. M., Mayer, B. W., Wei, Y., Devarakonda, R., Vose, R. S., & Cook, R. B. (2018). *Daymet: Daily Surface Weather Data on a 1-km Grid for North America, Version 3*. Oak Ridge, Tennessee, USA: ORNL DAAC. <https://doi.org/10.3334/ORNLDAA/1328>
- van den Hurk, B., Kim, H., Krinner, G., Seneviratne, S. I., Derksen, C., Oki, T., et al. (2016). LS3MIP (v1.0) contribution to CMIP6: The Land Surface, Snow and Soil moisture Model Intercomparison Project – aims, setup and expected outcome. *Geoscientific Model Development*, 9(8), 2809–2832. <https://doi.org/10.5194/gmd-9-2809-2016>
- Wahl, M., Follum, M., Snow, A., & Tavakoly, A. (2016). Developing hydrologic awareness. *The military engineer*, 108(700). Retrieved from. <http://themilitaryengineer.com/index.php/staging/item/556-march-april-2016>
- Wenger, S. J., Luce, C. H., Hamlet, A. F., Isaak, D. J., & Neville, H. M. (2010). Macroscale hydrologic modeling of ecologically relevant flow metrics. *Water Resources Research*, 46, W09513. <https://doi.org/10.1029/2009WR008839>
- Xiao, M., Udall, B., & Lettenmaier, D. P. (2018). On the causes of declining Colorado River streamflows. *Water Resources Research*, 54, 6739–6756. <https://doi.org/10.1029/2018WR023153>
- Yang, X., Thornton, P. E., Ricciuto, D. M., & Post, W. M. (2014). The role of phosphorus dynamics in tropical forests—A modeling study using CLM-CNP. *Biogeosciences*, 11(6), 1667–1681. <https://doi.org/10.5194/bg-11-1667-2014>
- Zhu, Z., Piao, S., Myneni, R. B., Huang, M., Zeng, Z., Canadell, J. G., et al. (2016). Greening of the Earth and its drivers. *Nature Climate Change*, 6(8), 791–795. <https://doi.org/10.1038/nclimate3004>